Chimeric PRMT6 protein produced by an endogenous retrovirus promoter regulates cell fate decision in mouse preimplantation embryos

Shinnosuke Honda, Maho Hatamura, Yuri Kunimoto, Shuntaro Ikeda, and Naojiro Minami

Laboratory of Reproductive Biology, Graduate School of Agriculture, Kyoto University, Kyoto 606-8502, Japan

Running Title: MERVL-PRMT6 regulates cell differentiation in mouse embryos.

Corresponding author: N Minami (e-mail: minami.naojirou.6r@kyoto-u.ac.jp)

Abstract

Murine endogenous retrovirus with leucine tRNA primer, also known as MERVL, is expressed during zygotic genome activation in mammalian embryos. Here we show that protein arginine N-methyltransferase 6 (*Prmt6*) forms a chimeric transcript with MT2B2, one of the long terminal repeat sequences of MERVL, and is translated into an elongated chimeric protein ($PRMT6^{MT2B2}$) whose function differs from that of the canonical PRMT6 protein ($PRMT6^{CAN}$) in mouse preimplantation embryos. Overexpression of $PRMT6^{CAN}$ in fibroblast cells increased asymmetric dimethylation of the third arginine residue of both histone H2A (H2AR3me2a) and histone H4 (H4R3me2a), while overexpression of $PRMT6^{MT2B2}$ increased only H2AR3me2a. In addition, overexpression of $PRMT6^{MT2B2}$ in one blastomere of mouse two-cell embryos promoted cell proliferation and differentiation of the blastomere into epiblast cells at the blastocyst stage, while overexpression of $PRMT6^{CAN}$ repressed cell proliferation. This is the first report of the translation of a chimeric protein ($PRMT6^{MT2B2}$) in mouse preimplantation embryos. Our results suggest that analyzing chimeric transcripts with MERVL will provide insight into the relationship between zygotic genome activation and subsequent intra- and extra-cellular lineage determination.

Key words: Mouse, endogenous retrovirus, *Prmt6*, preimplantation embryo,

development

33 **Introduction**

34 Immediately after fertilization, mammalian embryos have low transcriptional
35 activity and translate proteins from mRNA stored in oocytes. In mouse embryos,
36 transcription subsequently begins with two waves of zygotic genome activation (ZGA),
37 namely minor and major ZGA, the former during the S phase of the one-cell stage and
38 the latter during the late two-cell stage (Minami et al., 2007; Schulz and Harrison, 2019).
39 Before and after major ZGA, the epigenome of the fertilized egg changes dynamically
40 (Aoki, 2022; Burton and Torres-Padilla, 2010; Xu et al., 2021). Epigenetic modifications,
41 including DNA methylation and histone modifications, are known to be important for cell
42 differentiation during development (Wu and Sun, 2006). For example, *Carm1*, encoding
43 a protein arginine methyltransferase, has been reported to be involved in the
44 differentiation of blastomeres into epiblast cells through the dimethylation of histone
45 arginine residues in mouse preimplantation embryos (Torres-Padilla et al., 2007; White
46 et al., 2016). Endogenous retroviruses (ERVs) are one of the components of transposable
47 elements and occupy about 10% of human and mouse genomes (Ito et al., 2020; Mouse
48 Genome Sequencing Consortium, 2002). Although ERVs are among the earliest
49 transcribed genetic material in mouse preimplantation embryos (Kigami et al., 2003) and
50 various studies have shown that ERVs are expressed in mammalian preimplantation

51 embryos (Evsikov et al., 2004; Poznanski and Calarco; Wang et al., 2001), there is little
52 direct evidence that ERVs regulate cell differentiation. The high abundance of ERVs in
53 the mammalian genome (Ito et al., 2020) and the fact that several ERV-derived genes,
54 such as *Syncytin* and *Peg10*, are essential for placentation (Dupressoir et al., 2009;
55 Dupressoir et al., 2012; Mi et al., 2000; Suzuki et al., 2007) suggest that ERVs were
56 involved in the evolution of the placenta in mammals. Murine or human endogenous
57 retrovirus with leucine tRNA primer (MERVL or HERVL, respectively) is a transposable
58 element expressed during major ZGA in mice and humans (Franke et al., 2017; Kigami
59 et al., 2003; Macfarlan et al., 2012; Wang et al., 2001). It has been reported that MERVL-
60 activated mouse embryonic stem cells injected into eight-cell embryos can also contribute
61 to extra-embryonic tissues (Yang et al., 2020), suggesting that some MERVL/HERVL
62 elements may regulate the totipotency of mammalian embryos. Recently, a MERVL-
63 derived non-coding RNA called LincGET was shown to control the differentiation of
64 embryonic and extra-embryonic tissues in mouse preimplantation embryos (Wang et al.,
65 2018), but the function of the vast majority of MERVL elements remains to be elucidated.
66 Several studies have shown that the long terminal repeat of MERVL generates chimeric
67 transcripts with host genes during early embryonic development (Macfarlan et al., 2012;
68 Peaston et al., 2004). Because MERVL has been reported to be one of the earliest

transcribed genomic sequences in preimplantation embryos (Kigami et al., 2003; Wang et al., 2001), we hypothesized that MERVL chimeric transcripts contribute to the cell lineage differentiation that occurs after major ZGA (Chazaud and Yamanaka, 2016).

Reanalysis of previously reported RNA-sequencing (RNA-seq) data revealed that protein arginine N-methyltransferase 6 (*Prmt6*) expression is activated by the MERVL promoter sequence in preimplantation embryos. Like *Carm1*, *Prmt6* encodes a Type-I protein arginine methyltransferase (Di Lorenzo and Bedford, 2011) and has been shown to regulate the epigenome by the asymmetric di-methylation of arginine residues in histone proteins (Guccione et al., 2007; Hyllus et al., 2007; Kirmizis et al., 2007). Furthermore, overexpression or suppression of *Prmt6* in embryonic stem cells results in the loss of pluripotency and in the increased expression of differentiation marker genes (Lee et al., 2012). In the course of analyzing transcripts involved in MERVL in mouse preimplantation embryos, it was discovered that *Prmt6* has two transcripts of different lengths. One is the canonical *Prmt6* transcript ($Prmt6^{CAN}$), and the other is $Prmt6^{MT2B2}$, defined as the chimeric transcript of $Prmt6^{CAN}$ with MT2B2, the MERVL long terminal repeat sequence. It was also found that the chimeric transcript produced an elongated PRMT6 chimeric protein ($PRMT6^{MT2B2}$). In addition, the chimeric protein has different histone modification specificity from that of the canonical PRMT6 protein ($PRMT6^{CAN}$),

and overexpression of the chimeric protein in one blastomere of two-cell embryos promotes its contribution to the embryonic cell lineage. These findings shed light on a new aspect of the differentiation mechanism during embryogenesis.

91 **Results**

92 *Screening of candidate MERVL chimeric transcripts associated with cell lineage*
93 *differentiation*

94 Macfarlan et al. published a list of MERVL chimeric transcripts in mouse two-
95 cell stage embryos (Macfarlan et al., 2012), and we compared these transcripts with
96 histone modification–related genes (Fig. 1A). Although there was no statistically
97 significant bias, eight genes (*Atxn7*, *Brms1l*, *Ctcf*, *Kdm4c*, *Pcgf5*, *Prmt6*, *Rnf20*, and
98 *Smyd3*) overlapped, and half of them (*Ctcf*, *Kdm4c*, *Rnf20*, and *Smyd3*) had already been
99 reported to be important in early embryonic development (Ooga et al., 2015; Suzuki et
100 al., 2015; Wan et al., 2008; Wang et al., 2010). Analysis of a published RNA-seq dataset
101 (Zhang et al., 2016) revealed that the expression levels of four of the eight genes (*Ctcf*,
102 *Kdm4c*, *Pcgf5*, and *Prmt6*) were more than twice as high in late two-cell embryos
103 compared with early two-cell embryos (Fig. 1B)

104

105 *Expression dynamics of chimeric and canonical Prmt6 mRNA in mouse preimplantation*
106 *embryos*

107 Genomic analysis in mice revealed that MT2B2 is located 212 bp upstream of
108 the first exon of *Prmt6*, and that the chimeric transcript is transcribed from around 380 bp

109 upstream of the canonical transcription start site. To determine the expression profiles of
110 *Prmt6*^{MT2B2} and *Prmt6*^{CAN}, the amounts of total *Prmt6* transcripts (*Prmt6*^{MT2B2} and
111 *Prmt6*^{CAN}) and *Prmt6*^{MT2B2} during preimplantation development were determined by
112 quantitative RT-PCR (Fig. 2A). As expected, the amounts of total *Prmt6* transcripts and
113 *Prmt6*^{MT2B2} transcripts in the late two-cell stage were increased at major ZGA and
114 gradually decreased by the blastocyst stage (Fig. 2B). At the blastocyst stage, *Prmt6*^{MT2B2}
115 transcripts had almost completely disappeared, but *Prmt6*^{CAN} transcripts were still present,
116 albeit in small amounts (Fig. 2B). To compare the exact copy numbers of each transcript,
117 absolute quantification was performed using late two-cell embryos and blastocysts. In
118 late two-cell embryos, the amounts of total *Prmt6* transcripts and chimeric transcripts
119 were almost the same (Fig. 2C). In blastocysts, on the other hand, the copy number of
120 *Prmt6*^{MT2B2} transcripts was significantly lower than that of total *Prmt6* transcripts (Fig.
121 2C). Furthermore, microinjecting zygotes with si*Prmt6*^{MT2B2} (siRNA targeting the
122 sequence between the MT2B2 and *Prmt6*^{CAN} transcription start sites) or si*Prmt6*^{CAN}-1 or
123 si*Prmt6*^{CAN}-2 (siRNAs targeting the *Prmt6* exon sequence, see Fig. 2A) resulted in a
124 significant decrease in transcript levels of both total *Prmt6* transcripts and *Prmt6*^{MT2B2}
125 transcripts at the late two-cell stage (Fig. 2D). Since trimethylation of the fourth lysine
126 residue of histone H3 (H3K4me3) is generally increased around transcription start sites,

127 we analyzed the previously reported chromatin immunoprecipitation sequencing (ChIP-
128 seq) data of H3K4me3 (Liu et al., 2016) in preimplantation embryos and found that the
129 weak H3K4me3 ChIP-seq peak appeared at the MT2B2 region from the 2-cell stage and
130 became stronger at the 4-cell stage (Fig. 2E). On the other hand, the H3K4me3 peak at
131 just before the first exon of *Prmt6*^{CAN} was observed from the four-cell stage and get higher
132 at the eight-cell stage (Fig. 2E).
133
134 *Identification of the translation initiation codon of the PRMT6*^{MT2B2} *chimeric protein*
135 Since *Prmt6*^{MT2B2} has an extended sequence on the 5' side of *Prmt6*^{CAN} and two
136 putative translation initiation codons exist in this region, we sought to determine the site
137 where translation of the chimeric transcript began (Fig. 3A). Western blotting of the
138 PRMT6 protein using metaphase II (MII) oocytes and fertilized eggs at each
139 developmental stage revealed that ~55 kDa bands were detected in oocytes and embryos
140 during all developmental stages, and an additional ~42 kDa band was detected only in
141 embryos at the blastocyst stage (Fig. 3B). Since PRMT6^{CAN} has a molecular weight of
142 ~42 kDa, mRNAs of *Prmt6*^{CAN} and *Prmt6*^{MT2B2} were generated by in vitro transcription
143 to identify the translation product of the ~55 kDa protein detected at each developmental
144 stage. The mRNAs transfected into NIH3T3 cells revealed that *Prmt6*^{MT2B2} mRNA

145 encodes an elongated protein of ~55 kDa, while *Prmt6*^{CAN} mRNA encodes a protein of
146 ~42 kDa (Fig. 3C). Consistent with the amount of transcript, PRMT6^{MT2B2} with a
147 molecular weight of ~55 kDa was most abundant at the late two-cell stage and gradually
148 decreased until the blastocyst stage (Fig. 3B). There are two candidate translation
149 initiation codons (Met1 and Met2) for *Prmt6*^{MT2B2}, and Met3 is the translation initiation
150 codon for PRMT6^{CAN} (Fig. 3A). To determine which codon *Prmt6*^{MT2B2} is translated from,
151 three types of mRNAs mutated in Met1, Met2, or Met3 (AUG to AAG) were transfected
152 into NIH3T3 cells. Among NIH3T3 cells transfected with the three mutant mRNAs, only
153 those with the Met1 mutant transcript failed to produce the ~55 kDa PRMT6^{MT2B2} (Fig.
154 3C). The same results were obtained using mouse four-cell embryos (Fig. 3C). Bands at
155 ~55 kDa were detected in all four-cell embryos because these embryos express the
156 endogenous PRMT6^{MT2B2} (Fig. 3C). Knockdown of endogenous *Prmt6* transcripts with
157 siRNAs (si*Prmt6*^{CAN}-1 or si*Prmt6*^{CMT2B2}) at the one-cell stage decreased the amount of
158 the ~55 kDa protein at the four-cell stage (Fig. 3D).
159
160 *Functional analysis of the PRMT6*^{MT2B2} *chimeric protein*
161 Three-dimensional structure prediction using AlphaFold (Jumper et al., 2021)
162 showed no structural change in the S-adenosylmethionine–dependent methyltransferase

163 domain of PRMT6^{MT2B2} compared to PRMT6^{CAN} (Fig. 4A). Therefore, the ~55 kDa
164 PRMT6^{MT2B2} was considered to have arginine methylation activity, and the function of
165 this protein and its involvement in cell differentiation in mammalian preimplantation
166 embryos were examined. Since PRMT6^{CAN} is known to be a type I protein arginine
167 methyltransferase (Di Lorenzo and Bedford, 2011), western blotting was performed using
168 various histone arginine asymmetric dimethylation antibodies to confirm the histone
169 arginine methylation status of NIH3T3 cells overexpressing PRMT6^{CAN} or PRMT6^{MT2B2}.
170 Overexpression of PRMT6^{CAN} significantly increased asymmetric dimethylation of the
171 third arginine residue of both histone H2A (H2AR3me2a) and histone H4 (H4R3me2a)
172 (Fig. 4B, 4C, 4D). By contrast, overexpression of PRMT6^{MT2B2} significantly increased
173 only H2AR3me2a, while the amount is lower than overexpression of PRMT6^{CAN} (Fig.
174 4B, 4C, 4D; $P<0.01$).
175
176 *PRMT6^{MT2B2} regulates cell differentiation in mouse preimplantation embryos*
177 Analysis of published single cell RNA-seq data (Goolam et al., 2016) showed that
178 *Prmt6* is asymmetrically distributed among blastomeres in four- and eight-cell embryos
179 (Supplemental Fig. 1A). Next, we confirmed H2AR3me2a distribution among
180 blastomeres at each developmental stage. Immunostaining of H2AR3me2a showed an

181 asymmetrical distribution among blastomeres after the eight-cell stage and a greater
182 abundance in the trophectoderm (TE) than in the inner cell mass (ICM) at the blastocyst
183 stage (Supplemental Fig. 1B). *Prmt6*^{CAN} or *Prmt6*^{MT2B2} mRNA together with *H2B-EGFP*
184 mRNA as a lineage tracer was microinjected into one blastomere of two-cell embryos to
185 examine the effects on cell lineage specification in mouse preimplantation embryos (Fig.
186 5A). Overexpression of PRMT6^{MT2B2} significantly increased the number of H2B-EGFP–
187 positive cells in blastocysts at 96 h post insemination (hpi) compared to overexpression
188 of H2B-EGFP alone, while PRMT6^{CAN} overexpression reduced the number of H2B-
189 EGFP–positive cells in blastocysts at 96 hpi (Fig. 5B, 5C). In addition, overexpression of
190 PRMT6^{MT2B2} significantly increased the percentage of NANOG-positive epiblast cells in
191 H2B-EGFP–positive cells in blastocysts than overexpression of H2B-EGFP alone (Fig.
192 5B, 5D), while this percentage was unaffected by PRMT6^{CAN} overexpression (Fig. 5D).
193 The differentiation into trophectoderm (CDX2-positive cells) and primitive endoderm
194 (NANOG-negative and CDX2-negative cells) were not changed by PRMT6^{CAN} or
195 PRMT6^{MT2B2} overexpression (Supplementary Table 3). The si*Prmt6*^{CAN}-1 injection into
196 one blastomere of two-cell embryos resulted in the low number of H2B-EGFP–positive
197 cells in blastocyst, while neither si*Prmt6*^{CAN}-1 nor si*Prmt6*^{MT2B2} injection influence cell
198 differentiation (Supplementary Table 4). When *Prmt6*^{MT2B2} or *Prmt6*^{CAN} mRNA was

199 injected in one-cell embryos, cell numbers were not changed comparing with EGFP

200 mRNA injected control embryos, while the percentage of CDX2-positive cells was

201 decreased in PRMT6^{MT2B2} overexpressed embryos (Supplementary Table 5).

202

Discussion

Among the histone modification–related genes expressed as chimeric transcripts with MERVL, the expression of four genes (*Ctcf*, *Kdm4c*, *Pcgf5*, and *Prmt6*) dramatically increased during major ZGA, suggesting that many genes expressed during this period may be mainly under control of the MERVL promoter. Indeed, the results of absolute quantitative RT-PCR (Fig. 2C) and siRNA knockdown experiments targeting the intermediate sequence between MT2B2 and *Prmt6* exon (Fig. 2D) showed that almost all *Prmt6* transcripts were $Prmt6^{MT2B2}$ at the late two-cell stage. In contrast, most $Prmt6^{CAN}$ transcripts were expressed at the blastocyst stage, indicating that the transcriptional machinery of *Prmt6* is dramatically altered during early embryogenesis. Analysis of H3K4me3 ChIP-seq data supported the dynamic change of promoter activity, but the H3K4me3 peak at the MT2B2 region at the two-cell stage is weaker than the four- and eight-cell stage. The temporal mismatch between H3K4me3 ChIP-seq data and our quantitative RT-PCR data could be due to the difference of mice strain (Bertozzi et al., 2020) or collection time of 2-cell embryos.

Overexpression experiments of $Prmt6^{MT2B2}$ mRNA with a mutation in the translation initiation codon revealed that the $Prmt6^{MT2B2}$ chimeric transcript is translated into the $PRMT6^{MT2B2}$ chimeric protein from the 5'-extended uppermost ATG

221 codon (Fig. 3C, 3D). PRMT6^{MT2B2} is the first MERVL chimeric protein translated from
222 a chimeric transcript during mammalian development. Outside of early embryogenesis,
223 one case of a MERVL chimeric transcript translated into a longer protein was reported
224 in cancer cells (Lock et al., 2014). Since the extended 56-amino-acid sequence of
225 PRMT6^{MT2B2} showed no homology to retrovirus-derived proteins such as the GAG
226 protein (data not shown), further studies on the origin of the elongated sequence are
227 needed to understand the biological functions of PRMT6^{MT2B2} chimeric proteins.
228 Although many chimeric transcripts are expressed in cancer cells and embryonic stem
229 cells (Babaian and Mager, 2016; Macfarlan et al., 2012), their exact translation
230 initiation codons and biological functions remain unknown, and more comprehensive
231 proteomic analysis is needed to understand the precise function of chimeric transcripts,
232 including those expressed in preimplantation embryos.

233 Our results also revealed that the PRMT6^{MT2B2} chimeric protein has more
234 substrate-specific and/or lower histone arginine methylation activity than PRMT6^{CAN}
235 (Fig. 4B, 4C), suggesting that changes in epigenomic modifications may regulate
236 developmental progression and gene expression in early preimplantation embryos.
237 H2AR3me2a is asymmetrically distributed among blastomeres after the 8-cell stage and
238 is more abundant in trophectoderm at the blastocyst stage (Supplemental Fig. 1B). Since

239 PRMT6^{CAN} has a stronger ability to modify H2AR3me2a than PRMT6^{MT2B2} (Fig. 4C), it
240 is possible that the transcription shifts from *Prmt6^{MT2B2}* to *Prmt6^{CAN}* in some blastomeres
241 after the 8-cell stage, resulting in increased amounts of H2AR3me2a and enhanced
242 differentiation to trophectoderms. PRMT6 is known to be expressed in several cancer
243 tissues, including colorectal, breast, bladder, and lung adenocarcinomas (Avasarala et al.,
244 2020; Lim et al., 2018; Tang et al., 2020; Veland et al., 2017; Yoshimatsu et al., 2011).
245 Investigating how PRMT6^{MT2B2} is associated with cancer progression will provide insight
246 into the involvement of retroviruses in cancer development (Attermann et al., 2018;
247 Babaian and Mager, 2016; Kassiotis and Stoye, 2016; María et al., 2016) and a new
248 perspective on cancer research. The PRMT6^{CAN} protein contains a nuclear localization
249 signal (NLS) at the N-terminus (Fig. 3A) (Frankel et al., 2002; Herrmann et al., 2005).
250 Since it is known that the modification of surrounding amino acids and protein
251 conformation affect NLS function (Sorokin et al., 2007), it is possible that the extended
252 amino acid sequence of PRMT6^{MT2B2} leads to loss of NLS function and lower catalytic
253 activity for histone proteins. Since other arginine methyltransferases are known to
254 methylate proteins localized in the cytoplasm (Di Lorenzo and Bedford, 2011; Litt et al.,
255 2009), analysis of the subcellular localization of PRMT6^{MT2B2} could provide new insights
256 into its function.

257 In blastocysts, most *Prmt6* transcripts are presumably *Prmt6*^{CAN} based on
258 absolute quantification (Fig. 2C). Blastomeres overexpressing PRMT6^{MT2B2} were more
259 likely to consist of epiblast cells than non-injected blastomeres, while those
260 overexpressing PRMT6^{CAN} did not contribute to each cell lineage (Fig. 4G). In addition,
261 *Prmt6*^{MT2B2} mRNA microinjection to one-cell embryos showed lower CDX2-positive
262 cell rate at the blastocyst stage, which is stronger phenotype than *Prmt6*^{CAN} mRNA
263 injected embryos. These indicates that PRMT6^{MT2B2} and PRMT6^{CAN} have different
264 functions in cell differentiation during embryogenesis. It has been reported that
265 H3R2me2a mediated by PRMT6^{CAN} recruits Aurora B to chromosome arms (Kim et
266 al., 2020) and that overexpression of Aurora B facilitates cell contribution to the
267 placental cell lineage by regulating the nuclear dynamics of OCT4 in mouse
268 preimplantation embryos (Li et al., 2017; Plachta et al., 2011). Based on these results,
269 it is conceivable that an increased ratio of PRMT6^{CAN} to PRMT6^{MT2B2} promotes cell
270 differentiation during the blastocyst stage through localization of PRMT6^{CAN} in the
271 nucleus. In addition, several protein arginine methyltransferases have been reported to
272 act redundantly (Cheng et al., 2020; Wei et al., 2021). *Carm1* was found to promote
273 differentiation of blastomeres to epiblast cells via methylation of H3R26me2 (Goolam
274 et al., 2016; Torres-Padilla et al., 2007; White et al., 2016), and *Prmt1* enzymic inhibitor

275 promoted the differentiation of embryonic stem cells into primitive endoderm via Klf4
276 methylation (Zuo et al., 2022). These results support the possibility that PRMT6^{MT2B2},
277 but not PRMT6^{CAN}, may regulate the differentiation pathways in blastocysts.

278 Microinjection of PRMT6^{CAN} or si*Prmt6^{CAN}*-1 in a single blastomere in two-
279 cell stage embryos resulted in delayed cell proliferation (Fig. 4F), probably since
280 PRMT6^{CAN} controls the cell cycle, as reported in previous studies (Kim et al., 2020;
281 Schneider et al., 2021). On the other hand, overexpression of PRMT6^{MT2B2} promoted
282 cell proliferation (Fig. 4F), indicating that PRMT6^{CAN} and PRMT6^{MT2B2} affect cell
283 proliferation in different ways. Modzelewski et al. reported that the MERVL-*Cdk2ap1*
284 chimeric transcript is translated into a shorter protein (CDK2AP1$^{\Delta N}$) than the canonical
285 protein (CDK1AP1^{CAN}) in early mammalian embryos, and that CDK2AP1$^{\Delta N}$ promotes
286 cell proliferation while CDK2AP1^{CAN} inhibits the cell cycle (Modzelewski et al., 2021).
287 In mice, ZGA is known to occur earlier and to have a shorter implantation period than
288 in other mammals (Modzelewski et al., 2021). Adaptive evolution for rapid
289 development of mouse embryos may have occurred through the insertion of MT2B2
290 just before the Prmt6 locus, which allowed translation of the Prmt6MT2B2 chimeric
291 protein and may have promoted cell proliferation after ZGA. These findings and our
292 own indicate that chimeric transcripts expressed during major ZGA mediate different

293 functions than canonical transcripts.

294 In conclusion, we have shown that the chimeric transcript *Prmt6*^{MT2B2} is
295 expressed in mouse preimplantation embryos and that it generates the chimeric protein
296 PRMT6^{MT2B2} during major ZGA. Furthermore, PRMT6^{MT2B2} expressed in early
297 preimplantation embryos is involved in determining cell differentiation during the
298 blastocyst stage. This study reveals that MERVL expressed at major ZGA regulates cell
299 differentiation during embryogenesis by regulating the expression of nearby genes and
300 the translation of their corresponding mRNA.

301 **Materials and Methods**

302 *In vitro fertilization and embryo culture*

303 Eight- to twelve-week-old ICR female mice (Japan SLC, Hamamatsu, Japan)
304 were superovulated by injection of 7.5 IU of equine chorionic gonadotropin (eCG; ASKA
305 Pharmaceutical, Tokyo, Japan) followed by 7.5 IU of human chorionic gonadotropin
306 (hCG; ASKA Pharmaceutical) 48 h later. Cumulus oocyte complexes were harvested 14
307 h after hCG injection and placed in human tubal fluid (HTF) medium supplemented with
308 4 mg/ml bovine serum albumin (BSA, A3311; Sigma-Aldrich, St. Louis, MO) covered
309 with paraffin oil (Nacalai Tesque, Kyoto, Japan). Spermatozoa were collected from the
310 cauda epididymis of 13–20-week-old ICR male mice (Japan SLC) and cultured in HTF
311 medium for 1 h. After capacitation, sperm were introduced into oocyte-containing
312 droplets at a final concentration of 1×10^6 cells/ml. After 3-h incubation at 37°C in an
313 atmosphere of 5% CO_2, fertilized oocytes were washed with K^+-modified simplex
314 optimized medium (KSOM) supplemented with amino acids (Ho et al., 1995) and 1
315 mg/ml BSA, and then used for microinjection or cultured in the same medium under
316 paraffin oil at 37°C in an atmosphere of 5% CO_2 to the following stages: one-cell (12 h
317 post insemination (hpi)), early two-cell (24 hpi), late two-cell (36 hpi), four-cell (48 hpi),
318 eight-cell (54 hpi), morula (72 hpi), and blastocyst (96 hpi). MII oocytes were collected

319 from cumulus oocyte complexes followed by treatment with 1% hyaluronidase to remove

320 cumulus cells.

321

322 *Plasmid construction, in vitro transcription, and microinjection*

323 Based on the transcription start site of *Prmt6*^{CAN} predicted from the NCBI

324 database (NM_178891.5) and that of *Prmt6*^{MT2B2} predicted from previously reported

325 RNA-seq data (Liu et al., 2016), the sequences of *Prmt6*^{CAN} and *Prmt6*^{MT2B2} were cloned

326 by PCR from the cDNA of late two-cell embryos. The amplified products were digested

327 with EcoRI and XbaI, and the fragments were incorporated into a pBluescript II SK (−)

328 vector plasmid (Agilent Technologies Japan, Hachioji, Japan). Start codon mutant

329 constructs were generated by mutation PCR using the PrimeSTAR Mutagenesis Basal Kit

330 (Takara Bio, Kusatsu, Japan) by replacing AUG with AAG at Met1, Met2, or Met3. The

331 AAG codon was chosen because this mutation has been reported to cause complete loss

332 of translational activity in eukaryotic cells compared to other single-nucleotide mutations

333 (Wei et al., 2013). Methylase-inactive KLA mutant constructs were generated using the

334 same method by replacing amino acids Val–Leu–Asp at positions 89–91 in PRMT6^{CAN}

335 with Lys–Leu–Ala to produce PRMT^{CAN}-KLA (Boulanger et al., 2005), or by replacing

336 these amino acids at positions 145–147 in PRMT6^{MT2B2} with Lys–Leu–Ala to produce

337 PRMT6^{MT2B2}-KLA. Each mRNA was synthesized with the mMESSAGE mMECHINE
338 T7 Ultra Kit (Thermo Fisher Scientific, Waltham, MA), purified with the RNeasy Mini
339 Kit (Qiagen, Hilden, Germany), and then dissolved in nuclease-free water. For
340 knockdown experiments, siRNAs (RNAi, Tokyo, Japan) dissolved in nuclease-free water
341 at a concentration of 100 μM were used for microinjection. For overexpression
342 experiments, *Prmt6*^{CAN} or *Prmt6*^{MT2B2} mRNA was diluted to 250 ng/μl and co-injected
343 with *H2B-EGFP* mRNA at a concentration of 100 ng/μl. Approximately 5–10 pl of
344 mRNA or siRNA was microinjected into the cytoplasm of one-cell embryos at 3–5 hpi or
345 into the cytoplasm of one blastomere of two-cell embryos at 24–26 hpi in HEPES-
346 buffered KSOM. Microinjection was performed under an inverted microscope (IX73;
347 Olympus, Tokyo, Japan) equipped with a piezo injector (PMAS-CT150; PRIME TECH,
348 Tokyo, Japan) and a micromanipulator (IM-11-2; Narishige, Tokyo, Japan). The primers
349 and siRNA sequences are listed in Supplementary Tables 1 and 2.
350
351 *Cell culture and mRNA transfection*
352 NIH/3T3 cells were cultured in Dulbecco's modified Eagle's medium
353 supplemented with 10% calf serum, 75 μg/ml penicillin, and 50 μg/ml streptomycin.
354 mRNAs transcribed in vitro were transfected into 50–60% confluent cells using

Lipofectamine MessengerMAX Transfection Reagent (Thermo Fisher Scientific). Twenty-four hours after transfection, the cells were washed in phosphate-buffered saline (PBS) once and then lysed in 1X Laemmli sample buffer.

RNA extraction and quantitative RT-PCR

RNA extraction and reverse transcription were performed using the SuperPrep II Cell Lysis & RT Kit for qPCR (Toyobo, Osaka, Japan). Briefly, five embryos or oocytes were washed three times in PBS containing 0.5% polyvinylpyrrolidone (PVP K-30; Nacalai Tesque) (PVP-PBS) and collected in PCR tubes along with 0.5 µl of PVP-PBS. After adding 3.5 µl of lysate, all lysates were subjected to reverse transcription. Transcription levels were measured as previously described (Shikata et al., 2020) using the $2^{-\Delta\Delta Ct}$ method normalized against the corresponding *H2afz* levels (Jeong et al., 2014; Livak and Schmittgen, 2001). Absolute expression was determined using serial dilutions of the chimeric *Prmt6* cloned plasmid for in vitro transcription or using the pTAC plasmid in which an *H2afz* PCR fragment was cloned. The primers used for quantification are listed in Supplementary Table 2.

Western blotting

373 Fifty embryos or oocytes, excluding blastocysts, were washed three times in
374 PVP-PBS and collected in 1X Laemmli sample buffer. Twenty-five blastocysts were
375 collected. After boiling at 95°C for 5 min, the samples were kept at −80°C until use.
376 NIH3T3 cells were directly lysed in 1X Laemmli sample buffer. To analyze histone
377 arginine methylation modifications in NIH3T3 cells, TagRFP, PRMT6^{CAN}-KLA, or
378 PRMT6^{MT2B2}-KLA were used as negative controls for overexpression. Total protein was
379 separated by SDS–polyacrylamide gel electrophoresis (SDS-PAGE) and transferred into
380 a 0.22-μm-pore polyvinylidene fluoride (PVDF) membrane (Cytiva, Tokyo, Japan). After
381 one wash in PBS containing 0.1% Tween (PBST), the membrane was blocked in PBST
382 containing 5% BSA for 1 h at room temperature, followed by incubation with a rabbit
383 anti-PRMT6 antibody (1:1500 dilution; 15395-1-AP; Proteintech, Rosemont, IL), a rabbit
384 anti-H2AR3me2a antibody (1:1000 dilution; ab21574; Abcam, Cambridge, UK), a rabbit
385 anti-H4R3me2a antibody (1:500 dilution; 39706; Active Motif, Carlsbad, CA), a rabbit
386 anti-H3R2me2a antibody (1:1000 dilution; ab175007; Abcam), a rabbit anti-H3R8me2a
387 antibody (1:500 dilution; 39652; Active Motif), a rabbit anti-H3R17me2a antibody
388 (1:2000 dilution; 39710; Active Motif), a rabbit anti-H3R26me2 antibody (1:8000
389 dilution; 07-215; Merck, Darmstadt, Germany), a mouse anti–β-actin antibody (1:5000
390 dilution; A5441; Merck), or a rabbit anti–whole-H3 antibody (1:1000 dilution; #9715;

Cell Signaling, Danvers, MA) in PBST containing 1% BSA overnight at 4°C. After three washes in PBST, the membrane was incubated with a horseradish peroxidase–conjugated anti-mouse secondary antibody (1:10000 dilution; NA931; Cytiva) or anti-rabbit secondary antibody (1:10000 dilution; NA934; Cytiva) in PBST containing 1% BSA for 1 h at room temperature. After three washes in PBST, the membrane was developed using ImmunoStar LD (FUJIFILM Wako Pure Chemical Corporation, Osaka, Japan) and scanned with c-DiGit (LI-COR, Lincoln, NE). Densitometric quantification of the immunoblot bands was performed using Image Studio software (LI-COR).

Immunofluorescence

Embryos were fixed in PBS containing 4% paraformaldehyde for 20 min at 28°C. After three washes in PVP-PBS, embryos were permeabilized with 0.5% Triton X-100 (Sigma-Aldrich) in PBS for 40 min at 28°C. After washing three times in PVP-PBS, embryos were blocked in PBS containing 1.5% BSA, 0.02% Tween 20, and 0.2% sodium azide (blocking buffer) for 1 h at 28°C, and then incubated overnight at 4°C with a rabbit anti-NANOG antibody (1:100 dilution; RCAB002P-F; ReproCELL, Kanagawa, Japan) and a mouse anti-CDX2 antibody (1:100 dilution; MU392A-UC; Biogenex, Fremont, CA). After three washes in blocking buffer, embryos were incubated in blocking buffer

containing secondary antibodies (Alexa Fluor 555 donkey anti-rabbit IgG, 1:500 dilution, A31572, Thermo Fisher Scientific; Alexa Fluor 647 donkey anti-mouse IgG, 1:500 dilution, A31571, Thermo Fisher Scientific) for 1 h at 28°C. After washing three times in blocking buffer, nuclei were stained in blocking buffer containing 10 μg/ml Hoechst 33342 (Sigma-Aldrich) for 10 min at 28°C. Stained embryos were mounted on slide glass in blocking buffer containing 50% glycerol and signals were observed with a confocal fluorescent microscope (LSM880; Zeiss, Oberkochen, Germany). H2B-EGFP protein was detected based on its own fluorescence.

RNA-seq and ChIP-seq data processing

The bulk RNA-seq data (GSE71434) and the single cell RNA-seq data (E-MTAB-3321) of embryos of each stage were downloaded and then mapped to the mm10 with STAR (v. 2.7.10a) (Dobin et al., 2013). The gene expression level was estimated using RSEM (v. 1.3.3) (Li and Dewey, 2011) and normalized with the transcripts per kilobase million method. The H3K4me3 ChIP-seq data of mouse preimplantation embryos were downloaded from GSE73952 and mapped to the mm10 with bowtie2 (v. 2.4.5) (Langmead and Salzberg, 2012). In all cases, Bam files of biological replicates were merged using samtools (v. 1.10) (Li et al., 2009), normalized by counts per million

using deeptools (v. 3.5.1) (Ramírez et al., 2016), and visualized using Integrative Genomics Viewer software (v. 2.12.1) (Robinson et al., 2011).

Three-dimensional Structure Prediction of the PRMT6^{MT2B2} Protein

PRMT6^{CAN} and PRMT6^{MT2B2} protein structure prediction was performed using Alphafold (Jumper et al., 2021) on the Google Colaboratory site (https://colab.research.google.com/github/sokrypton/ColabFold/blob/main/AlphaFold2.ipynb). Obtained data were visualized using the Mol* site (Sehnal et al., 2021) (https://molstar.org/).

Statistical analyses

Quantitative RT-PCR data were analyzed by Student's t-test for pairwise comparisons or by Dunnett's test for multiple comparisons. Quantification of western blotting was performed using the Tukey-Kramer test. Cell contribution assays were analyzed with the Wilcoxon signed-rank test with holm's adjustment. All analyses were performed using R (v. 4.2.1), and significance was accepted at P-values < 0.05.

Ethical approval for the use of animals

All animal experiments were approved by the Animal Research Committee of Kyoto University (Permit Numbers: R3-17) and were performed in accordance with the committee's guidelines.

Competing interest statement

The authors declare no competing interests.

Acknowledgments

Confocal fluorescent microscopy was performed at the iCeMS Analysis Center, Institute for Integrated Cell-Material Sciences (iCeMS), Kyoto University Institute for Advanced Study (KUIAS). This work was supported by a Grant-in-Aid for Scientific Research (no. 19H03136 to N.M.) and a Grant-in-Aid for JSPS Fellows (no. 19J23290 to S.H.) from the Japan Society for the Promotion of Science.

Author contributions: The experiments were designed by S.H. and N.M., and were performed by S.H., with contributions from Y.K. and M.H. The manuscript was written by S.H. and N.M., with contributions from S.I. All authors read and approved the final manuscript.

References

Aoki, F. (2022). Zygotic gene activation in mice: profile and regulation. *J. Reprod. Dev.* **68**, 79–84.

Attermann, A. S., Bjerregaard, A.-M., Saini, S. K., Grønbæk, K. and Hadrup, S. R. (2018). Human endogenous retroviruses and their implication for immunotherapeutics of cancer. *Annals of Oncology* **29**, 2183–2191.

Avasarala, S., Wu, P.-Y., Khan, S. Q., Yanlin, S., Van Scoyk, M., Bao, J., Di Lorenzo, A., David, O., Bedford, M. T., Gupta, V., et al. (2020). PRMT6 Promotes Lung Tumor Progression via the Alternate Activation of Tumor-Associated Macrophages. *Molecular Cancer Research* **18**, 166–178.

Babaian, A. and Mager, D. L. (2016). Endogenous retroviral promoter exaptation in human cancer. *Mobile DNA* **7**, 24.

Bertozzi, T. M., Elmer, J. L., Macfarlan, T. S. and Ferguson-Smith, A. C. (2020). KRAB zinc finger protein diversification drives mammalian interindividual methylation variability. *Proc. Natl. Acad. Sci. U.S.A.* **117**, 31290–31300.

Boulanger, M.-C., Liang, C., Russell, R. S., Lin, R., Bedford, M. T., Wainberg, M. A. and Richard, S. (2005). Methylation of Tat by PRMT6 Regulates Human Immunodeficiency Virus Type 1 Gene Expression. *J Virol* **79**, 124–131.

480 **Burton, A. and Torres-Padilla, M.-E.** (2010). Epigenetic reprogramming and
481 development: a unique heterochromatin organization in the preimplantation
482 mouse embryo. *Briefings in Functional Genomics* **9**, 444–454.
483 **Chazaud, C. and Yamanaka, Y.** (2016). Lineage specification in the mouse
484 preimplantation embryo. *Development* **143**, 1063–1074.
485 **Cheng, D., Gao, G., Di Lorenzo, A., Jayne, S., Hottiger, M. O., Richard, S. and**
486 **Bedford, M. T.** (2020). Genetic evidence for partial redundancy between the
487 arginine methyltransferases CARM1 and PRMT6. *Journal of Biological*
488 *Chemistry* **295**, 17060–17070.
489 **Di Lorenzo, A. and Bedford, M. T.** (2011). Histone arginine methylation. *FEBS Letters*
490 **585**, 2024–2031.
491 **Dobin, A., Davis, C. A., Schlesinger, F., Drenkow, J., Zaleski, C., Jha, S., Batut, P.,**
492 **Chaisson, M. and Gingeras, T. R.** (2013). STAR: ultrafast universal RNA-seq
493 aligner. *Bioinformatics* **29**, 15–21.
494 **Dupressoir, A., Vernochet, C., Bawa, O., Harper, F., Pierron, G., Opolon, P. and**
495 **Heidmann, T.** (2009). Syncytin-A knockout mice demonstrate the critical role in
496 placentation of a fusogenic, endogenous retrovirus-derived, envelope gene. *Proc.*
497 *Natl. Acad. Sci. U.S.A.* **106**, 12127–12132.

498 **Dupressoir, A., Lavialle, C. and Heidmann, T.** (2012). From ancestral infectious
499 retroviruses to bona fide cellular genes: Role of the captured syncytins in
500 placentation. *Placenta* **33**, 663–671.
501 **Evsikov, A. V., de Vries, W. N., Peaston, A. E., Radford, E. E., Fancher, K. S., Chen,**
502 **F. H., Blake, J. A., Bult, C. J., Latham, K. E., Solter, D., et al.** (2004). Systems
503 biology of the 2-cell mouse embryo. *Cytogenet Genome Res* **105**, 240–250.
504 **Franke, V., Ganesh, S., Karlic, R., Malik, R., Pasulka, J., Horvat, F., Kuzman, M.,**
505 **Fulka, H., Cernohorska, M., Urbanova, J., et al.** (2017). Long terminal repeats
506 power evolution of genes and gene expression programs in mammalian oocytes
507 and zygotes. *Genome Res.* **27**, 1384–1394.
508 **Frankel, A., Yadav, N., Lee, J., Branscombe, T. L., Clarke, S. and Bedford, M. T.**
509 (2002). The Novel Human Protein Arginine N-Methyltransferase PRMT6 Is a
510 Nuclear Enzyme Displaying Unique Substrate Specificity. *Journal of Biological*
511 *Chemistry* **277**, 3537–3543.
512 **Goolam, M., Scialdone, A., Graham, S. J. L., Macaulay, I. C., Jedrusik, A.,**
513 **Hupalowska, A., Voet, T., Marioni, J. C. and Zernicka-Goetz, M.** (2016).
514 Heterogeneity in Oct4 and Sox2 Targets Biases Cell Fate in 4-Cell Mouse
515 Embryos. *Cell* **165**, 61–74.

516 **Guccione, E., Bassi, C., Casadio, F., Martinato, F., Cesaroni, M., Schuchlautz, H.,**
517 **Lüscher, B. and Amati, B.** (2007). Methylation of histone H3R2 by PRMT6 and
518 H3K4 by an MLL complex are mutually exclusive. *Nature* **449**, 933–937.
519 **Herrmann, F., Lee, J., Bedford, M. T. and Fackelmayer, F. O.** (2005). Dynamics of
520 Human Protein Arginine Methyltransferase 1(PRMT1) in Vivo. *Journal of*
521 *Biological Chemistry* **280**, 38005–38010.
522 **Ho, Y., Wigglesworth, K., Eppig, J. J. and Schultz, R. M.** (1995). Preimplantation
523 development of mouse embryos in KSOM: Augmentation by amino acids and
524 analysis of gene expression. *Mol. Reprod. Dev.* **41**, 232–238.
525 **Hyllus, D., Stein, C., Schnabel, K., Schiltz, E., Imhof, A., Dou, Y., Hsieh, J. and Bauer,**
526 **U.-M.** (2007). PRMT6-mediated methylation of R2 in histone H3 antagonizes H3
527 K4 trimethylation. *Genes Dev.* **21**, 3369–3380.
528 **Ito, J., Gifford, R. J. and Sato, K.** (2020). Retroviruses drive the rapid evolution of
529 mammalian *APOBEC3* genes. *Proc. Natl. Acad. Sci. U.S.A.* **117**, 610–618.
530 **Jeong, J.-K., Kang, M.-H., Gurunathan, S., Cho, S.-G., Park, C., Seo, H. G. and Kim,**
531 **J.-H.** (2014). Evaluation of reference genes in mouse preimplantation embryos
532 for gene expression studies using real-time quantitative RT-PCR (RT-qPCR).
533 *BMC Res Notes* **7**, 675.

Jumper, J., Evans, R., Pritzel, A., Green, T., Figurnov, M., Ronneberger, O., Tunyasuvunakool, K., Bates, R., Žídek, A., Potapenko, A., et al. (2021). Highly accurate protein structure prediction with AlphaFold. *Nature* **596**, 583–589.

Kassiotis, G. and Stoye, J. P. (2016). Immune responses to endogenous retroelements: taking the bad with the good. *Nat Rev Immunol* **16**, 207–219.

Kigami, D., Minami, N., Takayama, H. and Imai, H. (2003). MuERV-L Is One of the Earliest Transcribed Genes in Mouse One-Cell Embryos1. *Biology of Reproduction* **68**, 651–654.

Kim, S., Kim, N. H., Park, J. E., Hwang, J. W., Myung, N., Hwang, K.-T., Kim, Y. A., Jang, C.-Y. and Kim, Y. K. (2020). PRMT6-mediated H3R2me2a guides Aurora B to chromosome arms for proper chromosome segregation. *Nat Commun* **11**, 612.

Kirmizis, A., Santos-Rosa, H., Penkett, C. J., Singer, M. A., Vermeulen, M., Mann, M., Bähler, J., Green, R. D. and Kouzarides, T. (2007). Arginine methylation at histone H3R2 controls deposition of H3K4 trimethylation. *Nature* **449**, 928–932.

Langmead, B. and Salzberg, S. L. (2012). Fast gapped-read alignment with Bowtie 2. *Nat Methods* **9**, 357–359.

552 **Lee, Y. H., Ma, H., Tan, T. Z., Ng, S. S., Soong, R., Mori, S., Fu, X.-Y., Zernicka-**
553 **Goetz, M. and Wu, Q.** (2012). Protein Arginine Methyltransferase 6 Regulates
554 Embryonic Stem Cell Identity. *Stem Cells and Development* **21**, 2613–2622.
555 **Li, B. and Dewey, C. N.** (2011). RSEM: accurate transcript quantification from RNA-
556 Seq data with or without a reference genome.
557 **Li, H., Handsaker, B., Wysoker, A., Fennell, T., Ruan, J., Homer, N., Marth, G.,**
558 **Abecasis, G., Durbin, R., and 1000 Genome Project Data Processing**
559 **Subgroup** (2009). The Sequence Alignment/Map format and SAMtools.
560 *Bioinformatics* **25**, 2078–2079.
561 **Li, W., Wang, P., Zhang, B., Zhang, J., Ming, J., Xie, W. and Na, J.** (2017). Differential
562 regulation of H3S10 phosphorylation, mitosis progression and cell fate by Aurora
563 Kinase B and C in mouse preimplantation embryos. *Protein & Cell* **8**, 662–674.
564 **Lim, Y., Yu, S., Yun, J.-A., Do, I.-G., Cho, L., Kim, Y. H. and Kim, H. C.** (2018). The
565 prognostic significance of protein arginine methyltransferase 6 expression in
566 colon cancer. *Oncotarget* **9**, 9010–9020.
567 **Litt, M., Qiu, Y. and Huang, S.** (2009). Histone arginine methylations: their roles in
568 chromatin dynamics and transcriptional regulation. *Bioscience Reports* **29**, 131–
569 141.

570 **Liu, X., Wang, C., Liu, W., Li, J., Li, C., Kou, X., Chen, J., Zhao, Y., Gao, H., Wang,**
571 **H., et al.** (2016). Distinct features of H3K4me3 and H3K27me3 chromatin
572 domains in pre-implantation embryos. *Nature* **537**, 558–562.
573 **Livak, K. J. and Schmittgen, T. D.** (2001). Analysis of Relative Gene Expression Data
574 Using Real-Time Quantitative PCR and the 2−ΔΔCT Method. *Methods* **25**, 402–
575 408.
576 **Lock, F. E., Rebollo, R., Miceli-Royer, K., Gagnier, L., Kuah, S., Babaian, A.,**
577 **Sistiaga-Poveda, M., Lai, C. B., Nemirovsky, O., Serrano, I., et al.** (2014).
578 Distinct isoform of FABP7 revealed by screening for retroelement-activated genes
579 in diffuse large B-cell lymphoma. *Proc. Natl. Acad. Sci. U.S.A.* **111**,.
580 **Macfarlan, T. S., Gifford, W. D., Driscoll, S., Lettieri, K., Rowe, H. M., Bonanomi,**
581 **D., Firth, A., Singer, O., Trono, D. and Pfaff, S. L.** (2012). Embryonic stem cell
582 potency fluctuates with endogenous retrovirus activity. *Nature* **487**, 57–63.
583 **María, G.-C., Paola, I., Niki, K., Mariacarmela, S., Julià, B. and Rafael, R.** (2016).
584 Human endogenous retroviruses and cancer. *Cancer Biology & Medicine* **13**, 483.
585 **Mi, S., Lee, X., Li, X., Veldman, G. M., Finnerty, H., Racie, L., LaVallie, E., Tang,**
586 **X.-Y., Edouard, P., Howes, S., et al.** (2000). Syncytin is a captive retroviral
587 envelope protein involved in human placental morphogenesis. *Nature* **403**, 785–

588 789.

589 **Minami, N., Suzuki, T. and Tsukamoto, S.** (2007). Zygotic Gene Activation and

590 Maternal Factors in Mammals. *J. Reprod. Dev.* **53**, 707–715.

591 **Modzelewski, A. J., Shao, W., Chen, J., Lee, A., Qi, X., Noon, M., Tjokro, K., Sales,**

592 **G., Biton, A., Anand, A., et al.** (2021). A mouse-specific retrotransposon drives

593 a conserved Cdk2ap1 isoform essential for development. *Cell* **184**, 5541-5558.e22.

594 **Mouse Genome Sequencing Consortium** (2002). Initial sequencing and comparative

595 analysis of the mouse genome. *Nature* **420**, 520–562.

596 **Ooga, M., Suzuki, M. G. and Aoki, F.** (2015). Involvement of histone H2B

597 monoubiquitination in the regulation of mouse preimplantation development.

598 *Journal of Reproduction and Development* **61**, 179–184.

599 **Peaston, A. E., Evsikov, A. V., Graber, J. H., de Vries, W. N., Holbrook, A. E., Solter,**

600 **D. and Knowles, B. B.** (2004). Retrotransposons Regulate Host Genes in Mouse

601 Oocytes and Preimplantation Embryos. *Developmental Cell* **7**, 597–606.

602 **Plachta, N., Bollenbach, T., Pease, S., Fraser, S. E. and Pantazis, P.** (2011). Oct4

603 kinetics predict cell lineage patterning in the early mammalian embryo. *Nat Cell*

604 *Biol* **13**, 117–123.

605 **Poznanski, A. A. and Calarco, P. G.** The Expression of lntracisternal A Particle Genes

in the Preimplantation Mouse Embryo.

Ramírez, F., Ryan, D. P., Grüning, B., Bhardwaj, V., Kilpert, F., Richter, A. S., Heyne, S., Dündar, F. and Manke, T. (2016). deepTools2: a next generation web server for deep-sequencing data analysis. *Nucleic Acids Res* **44**, W160–W165.

Robinson, J. T., Thorvaldsdóttir, H., Winckler, W., Guttman, M., Lander, E. S., Getz, G. and Mesirov, J. P. (2011). Integrative genomics viewer. *Nat Biotechnol* **29**, 24–26.

Schneider, L., Herkt, S., Wang, L., Feld, C., Wesely, J., Kuvardina, O. N., Meyer, A., Oellerich, T., Häupl, B., Seifried, E., et al. (2021). PRMT6 activates cyclin D1 expression in conjunction with the transcription factor LEF1. *Oncogenesis* **10**, 42.

Schulz, K. N. and Harrison, M. M. (2019). Mechanisms regulating zygotic genome activation. *Nat Rev Genet* **20**, 221–234.

Sehnal, D., Bittrich, S., Deshpande, M., Svobodová, R., Berka, K., Bazgier, V., Velankar, S., Burley, S. K., Koča, J. and Rose, A. S. (2021). Mol* Viewer: modern web app for 3D visualization and analysis of large biomolecular structures. *Nucleic Acids Research* **49**, W431–W437.

Shikata, D., Yamamoto, T., Honda, S., Ikeda, S. and Minami, N. (2020). H4K20 monomethylation inhibition causes loss of genomic integrity in mouse

624 preimplantation embryos. *J. Reprod. Dev.* **66**, 411–419.

625 **Sorokin, A. V., Kim, E. R. and Ovchinnikov, L. P.** (2007). Nucleocytoplasmic transport

626 of proteins. *Biochemistry Moscow* **72**, 1439–1457.

627 **Suzuki, S., Ono, R., Narita, T., Pask, A. J., Shaw, G., Wang, C., Kohda, T., Alsop, A.**

628 **E., Marshall Graves, J. A., Kohara, Y., et al.** (2007). Retrotransposon Silencing

629 by DNA Methylation Can Drive Mammalian Genomic Imprinting. *PLoS Genet* **3**,

630 e55.

631 **Suzuki, S., Nozawa, Y., Tsukamoto, S., Kaneko, T., Imai, H. and Minami, N.** (2015).

632 Histone methyltransferase Smyd3 regulates early embryonic lineage commitment

633 in mice. *REPRODUCTION* **150**, 21–30.

634 **Tang, J., Meng, Q., Shi, R. and Xu, Y.** (2020). PRMT6 serves an oncogenic role in lung

635 adenocarcinoma via regulating p18. *Mol Med Rep*.

636 **Torres-Padilla, M.-E., Parfitt, D.-E., Kouzarides, T. and Zernicka-Goetz, M.** (2007).

637 Histone arginine methylation regulates pluripotency in the early mouse embryo.

638 *Nature* **445**, 214–218.

639 **Veland, N., Hardikar, S., Zhong, Y., Gayatri, S., Dan, J., Strahl, B. D., Rothbart, S.**

640 **B., Bedford, M. T. and Chen, T.** (2017). The Arginine Methyltransferase PRMT6

641 Regulates DNA Methylation and Contributes to Global DNA Hypomethylation in

Cancer. *Cell Reports* **21**, 3390–3397.

Wan, L.-B., Pan, H., Hannenhalli, S., Cheng, Y., Ma, J., Fedoriw, A., Lobanenkov, V., Latham, K. E., Schultz, R. M. and Bartolomei, M. S. (2008). Maternal depletion of CTCF reveals multiple functions during oocyte and preimplantation embryo development. *Development* **135**, 2729–2738.

Wang, Q., Chung, Y. G., deVries, W. N., Struwe, M. and Latham, K. E. (2001). Role of Protein Synthesis in the Development of a Transcriptionally Permissive State in One-Cell Stage Mouse Embryos1. *Biology of Reproduction* **65**, 748–754.

Wang, J., Zhang, M., Zhang, Y., Kou, Z., Han, Z., Chen, D.-Y., Sun, Q.-Y. and Gao, S. (2010). The Histone Demethylase JMJD2C Is Stage-Specifically Expressed in Preimplantation Mouse Embryos and Is Required for Embryonic Development1. *Biology of Reproduction* **82**, 105–111.

Wang, J., Wang, L., Feng, G., Wang, Y., Li, Y., Li, X., Liu, C., Jiao, G., Huang, C., Shi, J., et al. (2018). Asymmetric Expression of LincGET Biases Cell Fate in Two-Cell Mouse Embryos. *Cell* **175**, 1887-1901.e18.

Wei, J., Zhang, Y., Ivanov, I. P. and Sachs, M. S. (2013). The Stringency of Start Codon Selection in the Filamentous Fungus Neurospora crassa. *Journal of Biological Chemistry* **288**, 9549–9562.

660 **Wei, H.-H., Fan, X.-J., Hu, Y., Tian, X.-X., Guo, M., Mao, M.-W., Fang, Z.-Y., Wu,**
661 **P., Gao, S.-X., Peng, C., et al.** (2021). A systematic survey of PRMT interactomes
662 reveals the key roles of arginine methylation in the global control of RNA splicing
663 and translation. *Science Bulletin* **66**, 1342–1357.
664 **White, M. D., Angiolini, J. F., Alvarez, Y. D., Kaur, G., Zhao, Z. W., Mocskos, E.,**
665 **Bruno, L., Bissiere, S., Levi, V. and Plachta, N.** (2016). Long-Lived Binding of
666 Sox2 to DNA Predicts Cell Fate in the Four-Cell Mouse Embryo. *Cell* **165**, 75–
667 87.
668 **Wu, H. and Sun, Y. E.** (2006). Epigenetic Regulation of Stem Cell Differentiation.
669 *Pediatr Res* **59**, 21R-25R.
670 **Xu, R., Li, C., Liu, X. and Gao, S.** (2021). Insights into epigenetic patterns in
671 mammalian early embryos. *Protein Cell* **12**, 7–28.
672 **Yang, F., Huang, X., Zang, R., Chen, J., Fidalgo, M., Sanchez-Priego, C., Yang, J.,**
673 **Caichen, A., Ma, F., Macfarlan, T., et al.** (2020). DUX-miR-344-ZMYM2-
674 Mediated Activation of MERVL LTRs Induces a Totipotent 2C-like State. *Cell*
675 *Stem Cell* **26**, 234-250.e7.
676 **Yoshimatsu, M., Toyokawa, G., Hayami, S., Unoki, M., Tsunoda, T., Field, H. I.,**
677 **Kelly, J. D., Neal, D. E., Maehara, Y., Ponder, B. A. J., et al.** (2011).

Dysregulation of PRMT1 and PRMT6, Type I arginine methyltransferases, is involved in various types of human cancers. *Int. J. Cancer* **128**, 562–573.

Zhang, B., Zheng, H., Huang, B., Li, W., Xiang, Y., Peng, X., Ming, J., Wu, X., Zhang, Y., Xu, Q., et al. (2016). Allelic reprogramming of the histone modification H3K4me3 in early mammalian development. *Nature* **537**, 553–557.

Zuo, Z., Yang, G., Wang, H., Liu, S., Zhang, Y., Cai, Y., Chen, F., Dai, H., Xiao, Y., Cheng, M., et al. (2022). Klf4 methylated by Prmt1 restrains the commitment of primitive endoderm. *Nucleic Acids Research* **50**, 2005–2018.

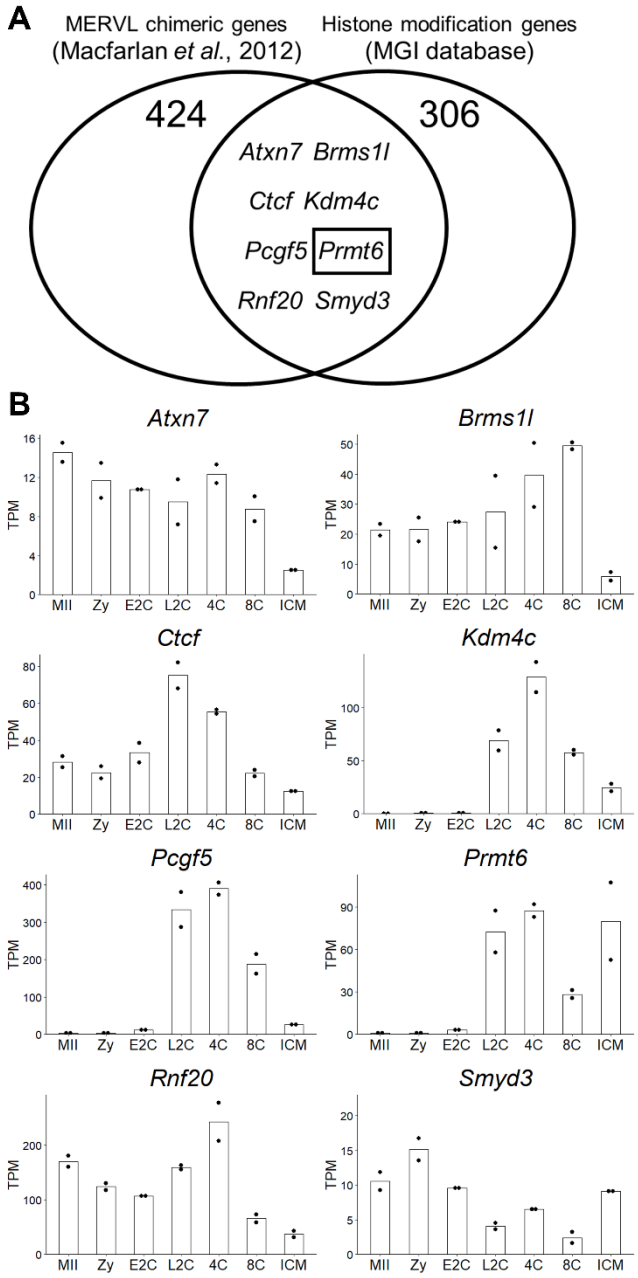

688

689 **Fig. 1.** Verification of MERVL-mediated chimeric genes.

690 (A) Venn diagram showing overlap of genes expressed as chimeric transcripts with

691 MERVL- and histone modification–related genes. The list of MERVL chimeric genes

692 were obtained from published data (Macfarlan et al., 2012), and the list of histone

693 modification-related genes were obtained from MGI database

694 (http://www.informatics.jax.org) in Jan. 2019. (B) The expression patterns of eight

695 overlapping genes in MII oocytes and preimplantation embryos. Dots represent

696 replicates. Data were obtained from GSE71434. MII: MII oocytes, Zy: zygotes, E2C:

697 early two-cell embryos, 4C: four-cell embryos, 8C: eight-cell embryos, ICM: inner cell

698 mass cells.

699

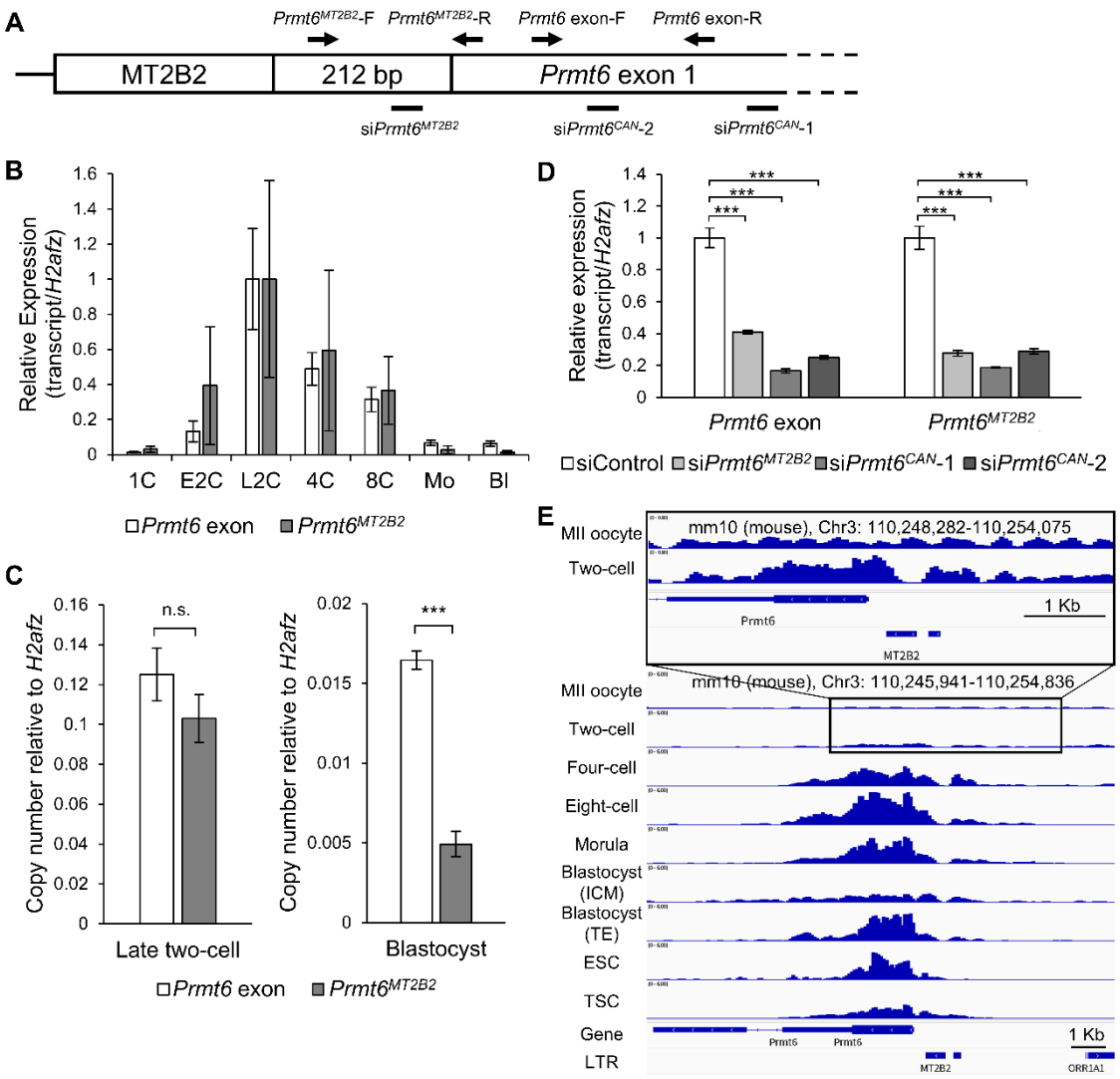

700

701 **Fig. 2.** Gene structure and transcriptional profile of *Prmt6* in mice.

702 (A) Schematic diagram showing the positions of MT2B2 and *Prmt6* in the mouse

703 genome. MT2B2 is located 212 bp upstream from the transcription start site of *Prmt6*.

704 The names of primers and targeting loci (arrows) are indicated above the diagram, and

705 the names of siRNAs and their targeting sites (bars) are indicated underneath. (B) qRT-

706 PCR analysis of the *Prmt6* exon and *Prmt6*^{MT2B2} transcripts during mouse

707 preimplantation development. The amount of mRNA in one-cell embryos was defined
708 as 1, and the expression levels were normalized to *H2afz* as an internal control. Data
709 are expressed as mean ± s.e.m. (n=3). (C) Comparison of expression levels of the *Prmt6*
710 exon and *Prmt6*^{MT2B2} in late two-cell embryos and blastocysts based on absolute
711 quantification by qRT-PCR. Each graph shows the expression levels of each transcript
712 in late two-cell embryos and blastocysts. Copy numbers were normalized to *H2afz* copy
713 numbers. Data are expressed as mean ± s.e.m. (n=5). Student's t-test, ***P < 0.001;
714 n.s., not significant. (D) qRT-PCR analysis of *Prmt6* and *Prmt6*^{MT2B2} mRNA abundance
715 in embryos injected with si*Prmt6*^{MT2B2}, si*Prmt6*-1, si*Prmt6*-2, or siControl in the late
716 two-cell stage. Injection was performed 3–5 h after IVF. The amount of mRNA in
717 siControl-injected embryos was defined as 1, and the expression levels were
718 normalized to *H2afz* as an internal control. Data are expressed as mean ± s.e.m. (n=3).
719 Dunnett's test, ***P < 0.001. (E) Genome browser view of H3K4me3 ChIP-seq data
720 from each stage of mouse preimplantation embryos. Data for MII oocytes, two-cell
721 embryos, four-cell embryos, eight-cell embryos, morulae, inner cell mass (ICM) and
722 trophectoderm (TE) of blastocysts, embryonic stem cells (ESC), and trophoblast stem
723 cells (TSC) are shown. The *Prmt6*^{CAN} exon and MT2B2 locations are indicated at the
724 bottom. Data were obtained from GSE73952. A magnified view of the data for MII

725 oocytes and two-cell embryos are shown in the upper panel.

726 1C: one-cell embryo, E2C: early two-cell embryo, L2C: late two-cell embryo, 4C: four-

727 cell embryo, 8C: eight-cell embryo, Mo: morula, Bl: blastocyst

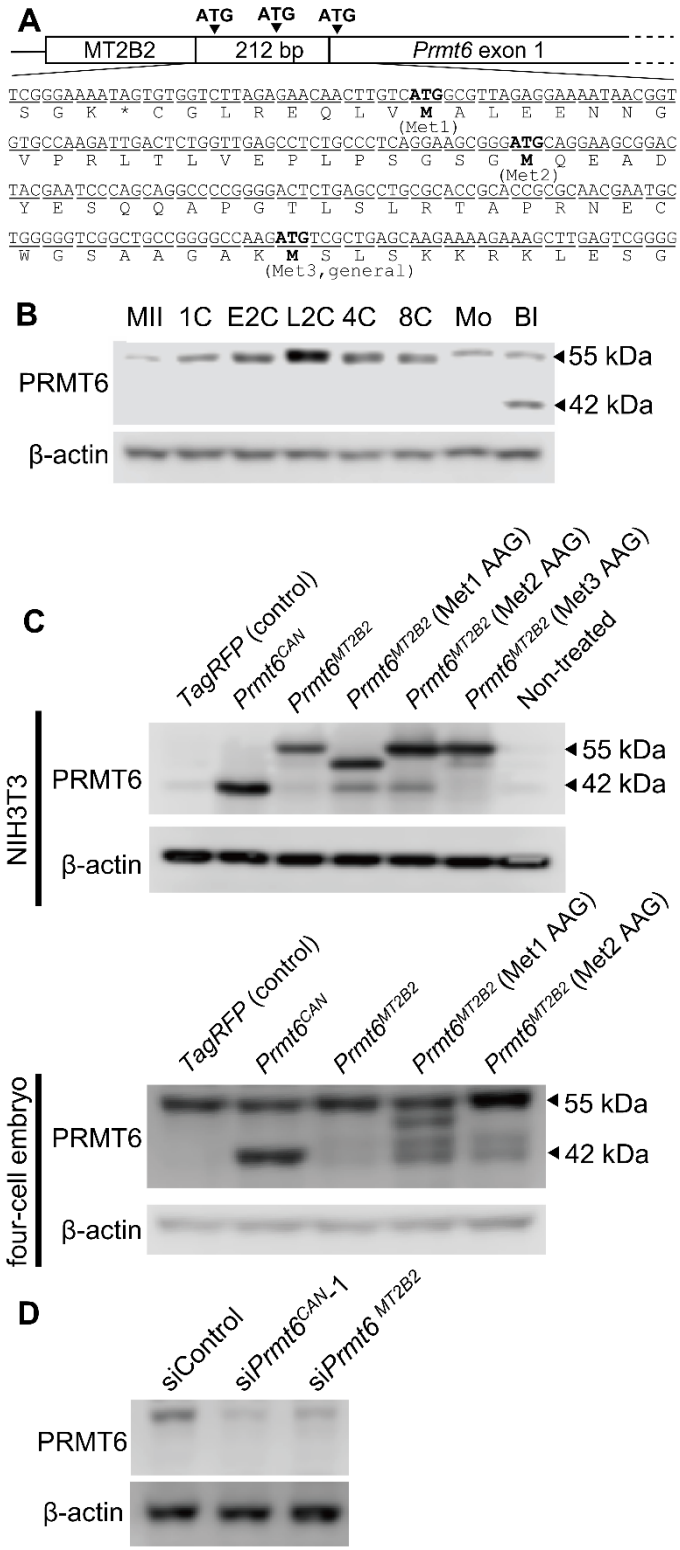

Fig. 3. Protein expression of Prmt6.

730 (A) Schematic diagram of the genome structure (upper) and genome and protein
731 sequences (lower) of *Prmt6* exon 1. Candidate translation initiation codons (Met1 and
732 Met2) and the canonical translation initiation codon (Met3) are indicated above the
733 schematic diagram and are shown in bold in the sequences. (B) Western blotting of
734 PRMT6 in mouse oocytes and preimplantation embryos. β-actin was used as a loading
735 control. Fifty oocytes or embryos were used in each lane except blastocysts. Twenty-
736 five blastocysts were used. The approximate molecular weight is on the right. The
737 representative result is shown from three independent experiments. (C) Western
738 blotting analysis for PRMT6 in NIH3T3 cells and four-cell embryos. NIH3T3 cells
739 were transfected with TagRFP mRNA, *Prmt6*^{CAN} mRNA, *Prmt6*^{MT2B2} mRNA,
740 *Prmt6*^{MT2B2} with Met1 mutant mRNA (Met1 AAG), *Prmt6*^{MT2B2} with Met2 mutant
741 mRNA (Met2 AAG), or *Prmt6*^{MT2B2} with Met3 mutant mRNA (Met3 AAG). Zygotes
742 were injected with the same mRNAs except *Prmt6*^{MT2B2} with Met3 mutant mRNA
743 (Met3 AAG) and cultured to the four-cell stage. Fifty embryos were used in each lane.
744 β-actin was used as a loading control. The approximate molecular weight is on the right.
745 The representative result is shown from three independent experiments. (D) Western
746 blotting analysis of PRMT6 protein in Prmt6-suppressed four-cell embryos.
747 si*Prmt6*^{CAN}-1, si*Prmt6*^{MT2B2}, or siControl was injected into zygote cytoplasm. β-actin

748 was used as a loading control. Fifty embryos were used for each lane. The approximate
749 molecular weight is on the right. The representative result is shown from three
750 independent experiments.
751 MII: metaphase II oocyte, 1C: one-cell embryo, E2C: early two-cell embryo, L2C: late
752 two-cell embryo, 4C: four-cell embryo, 8C: eight-cell embryo, Mo: morula, Bl:
753 blastocyst
754

755

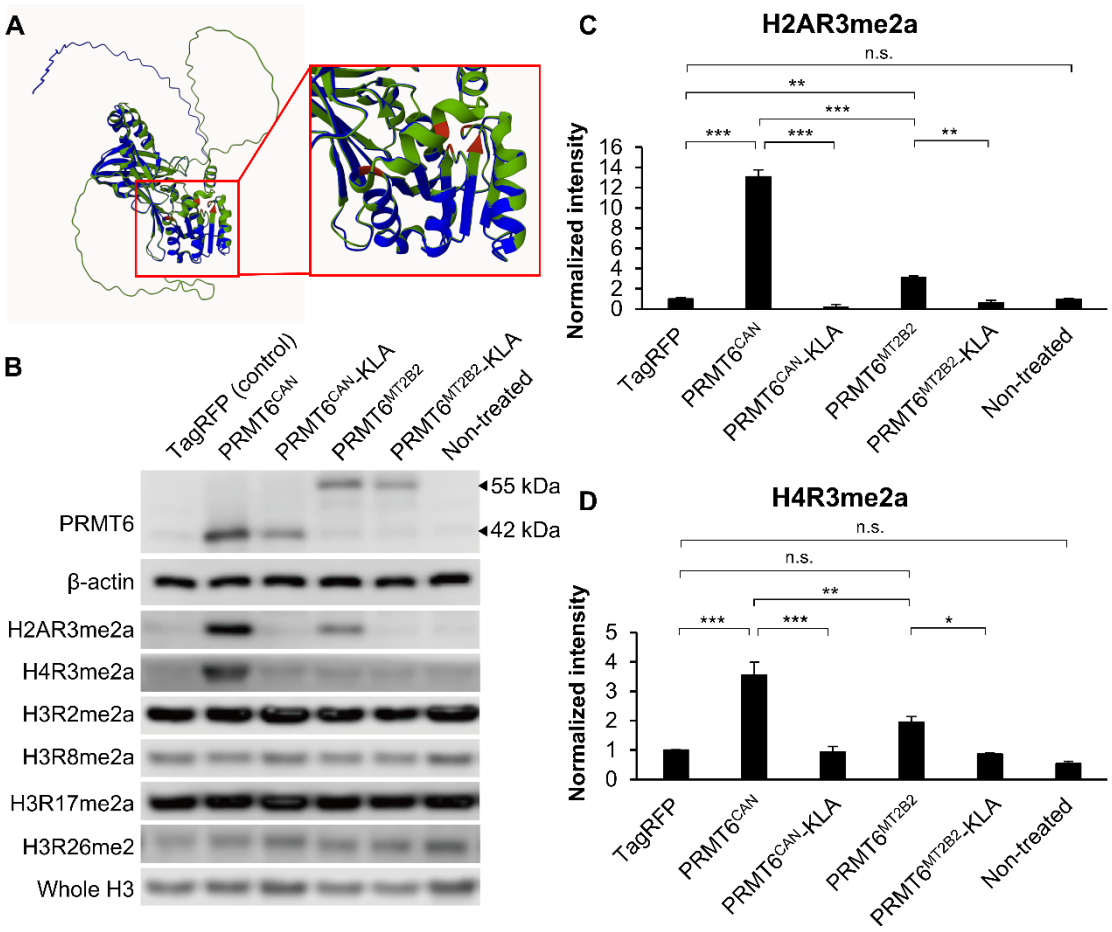

756

757 **Fig. 4.** Substrate-specific histone arginine methylation activity of PRMT6^{MT2B2}.

758 (A) The 3D structures of PRMT6^{CAN} and PRMT6^{MT2B2} as predicted by AlphaFold2.

759 The blue structure represents PRMT6^{CAN} and the green structure represents

760 PRMT6^{MT2B2}. The five S-adenosylmethionine binding sites are shown in red. The right

761 panel shows a magnified view of the catalytic domain. (B) Western blotting analysis of

762 various histone arginine methylation modifications in NIH3T3 cells overexpressing

763 TagRFP, PRMT6^{CAN}, PRMT6^{CAN}-KLA, PRMT6^{MT2B2}, or PRMT6^{MT2B2}-KLA. β-actin

764 and whole H3 were used as loading controls. KLA-containing proteins are those in

765 which the enzyme activity is eliminated by replacing amino acids VLD with KLA. (C,

766 D) The amounts of H2AR3me2 (C) and H4R3me2 (D) based on the intensity

767 of (B). Overexpression of $PRMT6^{CAN}$ increases H2AR3me2a and H4R3me2a intensity,

768 while overexpression of $PRMT6^{MT2B2}$ increases only H2AR3me2a intensity. Data are

769 expressed as mean ± s.d. (n=3). Tukey-Kramer test, ***P < 0.001; **P < 0.01; *P <

770 0.05; n.s., not significant.

771

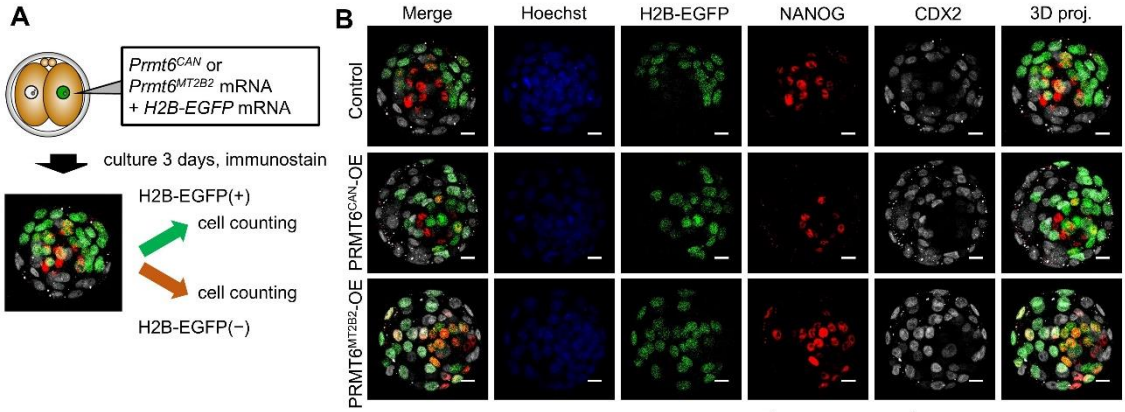

C

	Blastocysts 3D	Total cells (n)	NANOG⁺ cells (%)	GFP⁺ cells (%)	NANOG⁺ cells that are GFP⁺ (%)	NANOG⁺ cells that are GFP⁻ (%)	GFP⁺ cells that are NANOG⁺ (%)
H2B-EGFP control	55	78.47 ± 13.69	(11.09 ± 5.34)	(48.63 ± 7.96)	(12.30 ± 7.61)	(10.39 ± 7.68)	(53.70 ± 23.92)
PRMT6^{CAN}-OE	49	75.00 ± 16.28	(12.09 ± 5.65)	(43.81 ± 8.56)*	(14.54 ± 11.14)	(10.26 ± 5.85)	(49.08 ± 23.97)
PRMT6^{MT2B2}-OE	58	75.83 ± 14.49	(13.44 ± 6.19)*	(51.77 ± 8.44)*	(15.65 ± 8.54)*	(10.87 ± 7.15)	(60.82 ± 21.92)

772

773 **Fig. 5.** PRMT6^{MT2B2} determines the cell fate of mouse preimplantation embryos.

774 (A) Schematic view of the cell fate contribution assay. *Prmt6^{CAN}* or *Prmt6^{MT2B2}* mRNA

775 together with *H2B-EGFP* mRNA was microinjected into one blastomere of two-cell

776 embryos. Embryos cultured until the blastocyst stage (96 hpi) were subjected to

777 immunostaining using antibodies against NANOG (red) and CDX2 (white). Cell nuclei

778 were stained with Hoechst (blue). The number of NANOG-positive cells was counted

779 separately for H2B-EGFP–positive and –negative cells. (B) Immunostaining of

780 NANOG and CDX2 in blastocysts overexpressing H2B-EGFP (control), PRMT6^{CAN}

781 with H2B-EGFP (PRMT6^{CAN}-OE), or PRMT6^{MT2B2} with H2B-EGFP (PRMT6^{MT2B2}-

782 OE). Photos are representative of immunostained blastocysts. Hoechst (blue), H2B-

783 EGFP (marker, green), NANOG (red), CDX2 (white), and 3D maximum projections of

784 merged images are shown. Scale bars, 20 μm. (C) Analysis of the distribution of
785 progeny of injected blastomere at the blastocyst stage based on (B). Data were
786 represented as mean ±s.d. Wilcoxon signed-rank test with holm's adjustment were used
787 for statistical analysis, *$P < 0.05$. Seven experimental replicates were performed. Key
788 to table headings: Blastocysts 3D is the number of blastocysts that were all analyzed,
789 Total cells (n) is the total number of cells in the blastocyst, $NANOG^+$ cells (%) is the
790 percentage of NANOG-positive cells out of the total number of cells in the blastocyst,
791 GFP^+ cells (%) is the percentage of GFP-positive cells out of the total number of cells
792 in the blastocyst, $NANOG^+$ cells that are GFP^+ (%) is the percentage of NANOG-
793 positive cells out of the total number of GFP-positive cells in the blastocyst, $NANOG^+$
794 cells that are GFP^- (%) is the percentage of NANOG-positive cells out of the total
795 number of GFP-negative cells in the blastocyst, and GFP^+ cells that are $NANOG^+$ (%)
796 is the percentage of GFP-positive cells out of the total number of NANOG-positive
797 cells in the blastocyst.

Supplementary Information for

Chimeric protein of PRMT6 produced by endogenous retrovirus promoter regulates cell fate decision in mouse preimplantation embryos

Shinnosuke Honda, Maho Hatamura, Yuri Kunimoto, Shuntaro Ikeda, and Naojiro Minami*

Laboratory of Reproductive Biology, Graduate School of Agriculture, Kyoto University, Kyoto 606-8502, Japan

*Corresponding author

Email: minami.naojirou.6r@kyoto-u.ac.jp

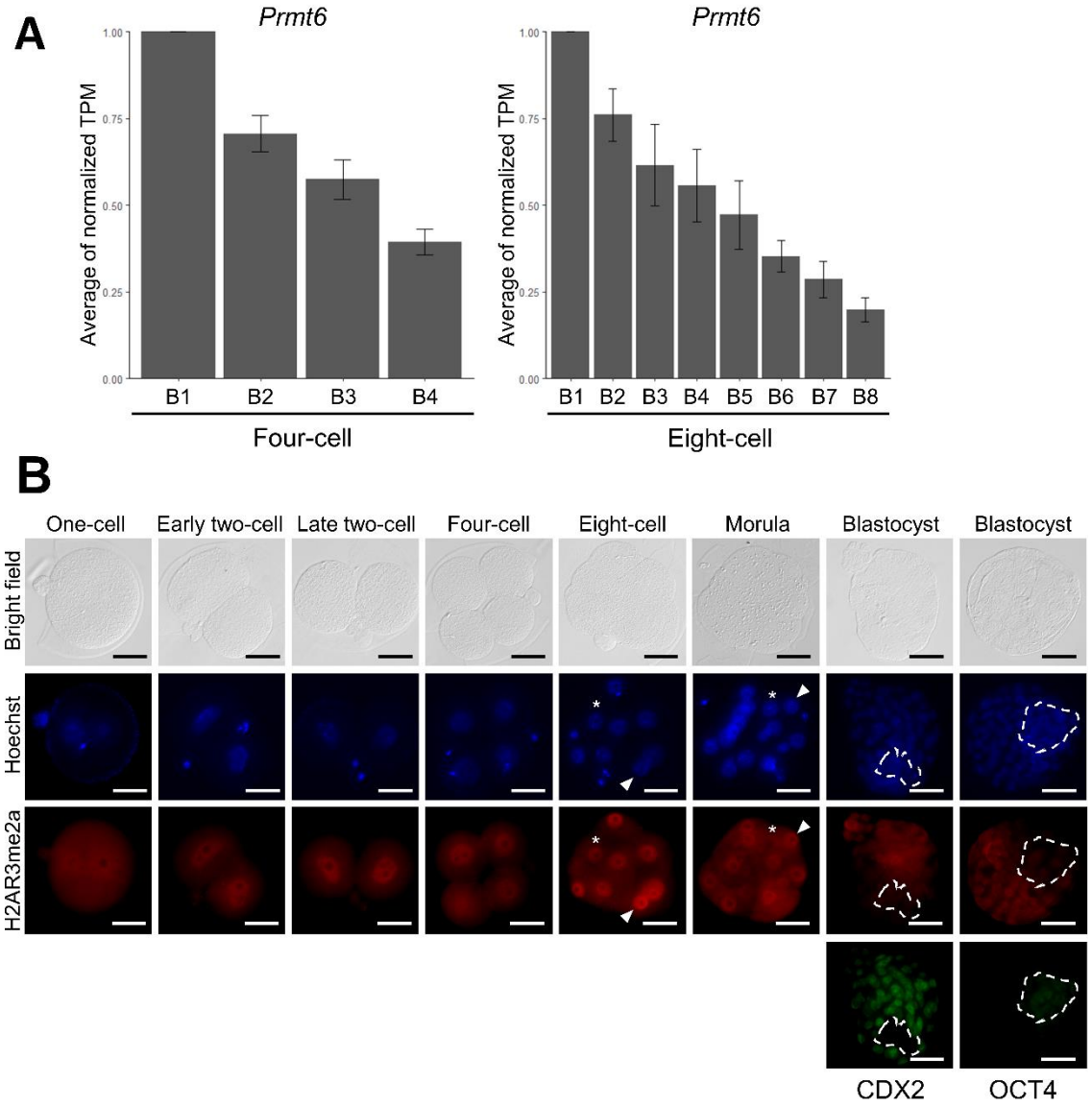

Supplementary Fig. 1. Asymmetric distribution of *Prmt6* mRNA and H2AR3me2a.

(A) Average of the relative *Prmt6* mRNA levels in each blastomere at four- and eight-cell stage. Each blastomere at 4- or 8-cell stage is named B1 to B4 (4-cell, n=16) or B1 to B8 (8-cell, n=4) according to the amount of *Prmt6* expression. TPM (Transcripts Per Million) was normalized based on the blastomere with highest *Prmt6* expression in each embryo, and the mean averages are shown (± s.e.m.). Data were obtained from E-MTAB-3321. (B) Immunostaining for H2AR3me2a in embryos at each developmental stage. Hoechst (blue), H2AR3me2a (red), and CDX2 or OCT4 (green, only at the blastocyst stage) are shown. Scale bars, 50 μm. Arrowheads indicate the cell with high fluorescence and asterisks indicate the cell with low fluorescence in four- and eight-cell embryos. Dotted lines mark the inner cell mass in blastocysts.

Supplementary Table 1. Sequences of siRNAs used for microinjection

Names of siRNAs	Sense Strand (5'→3')	Antisense Strand (5'→3')
si*Prmt6* ^{MT2B2}	GCCAAGAUUGACUCUGGUUdTdT	AACCAGAGUCAAUCUUGGCdTdT
si*Prmt6* ^{CAN} -1	GCCGUCUGGUUUCAAGUGAdCdC	UCACUUGAAACCAGACGGCdGdG
si*Prmt6* ^{CAN} -2	CACCGAAGCCUACCGCUUAdGdG	UAAGCGGUAGGCUUCGGUGdCdC
siControl	GUACCGCACGUCAUUCGUAUC	UACGAAUGACGUGCGGUACGU

dT, 2'-deoxythymidine; dC, 2'-deoxycytidine; dG, 2'-deoxyguanosine

Supplementarry Table 2. Primer sequences

for quantitative PCR			
Primer names		Sequences	Product sizes (bp)
Prmt6 exon	sense	AGTGCTACTCCGACGTCTCG	149
	anti-sense	GATGCTGAGAATGCCGGTGC	
Prmt6^{MT2B2}	sense	AGGGGTAAAAGGAAAGGGCAA	278
	anti-sense	GTCCCCCGACTCAAGCTTTC	
H2afz	sense	GGTAAAGCGTATCACCCCTCG	130
	anti-sense	CTTCCCGATCAGCGATTTGTG	
for plasmid construction			
Primer names		Sequences	Product sizes (bp)
Prmt6^{MT2B2} cloning	sense	AAAGAATTCAGAGAACCCTGACAAGGGGTA	1408
	anti-sense	AAATCTAGATCAGTCCTCCATGGCAAAGTC	
Prmt6^{CAN} cloning	sense	AAAGAATTCATGTCGCTGAGCAAGAAAAGAA	1155
	anti-sense	AAATCTAGATCAGTCCTCCATGGCAAAGTC	
Met1 mutation	sense	CTTGTCAAGGCGTTAGAGGAAAATAA	–
	anti-sense	TAACGCCTTGACAAGTTGTTCTCTAA	
Met2 mutation	sense	AGCGGGAAGCAGGAAGCGGACTACGA	–
	anti-sense	TTCCTGCTTCCCGCTTCCTGAGGGCA	
Met3 mutation	sense	GCCAAGAAGTCGCTGAGCAAGAAAAG	–
	anti-sense	CAGCGACTTCTTGGCCCCGGCAGCCG	
KLA mutation	sense	ACGAAGCTTGCGGTGGGCGCGGGCACCGGC	–
	anti-sense	CACCGCAAGCTTCGTCTTGCCTCGCAGCGC	
for in vitro transcription			
Primer names		Sequences	Product sizes (bp)
Prmt6^{CAN}, *Prmt6*^{MT2B2} IVT	sense	TAAGTTGGGTAACGCCAGGG	1351, 1604
	anti-sense	AGCGCGCAATTAACCCTCAC	
H2B-EGFP IVT	sense	TAAGTTGGGTAACGCCAGGG	1501
	anti-sense	GGAGCAGATACGAATGGCTACA	

Supplementary Table 3. Analysis of the distribution of progeny of injected blastomere at the blastocyst stage based on Fig. 5B.

	Blastocysts 3D	$CDX2^+$ cells (%)	$CDX2^+$ cells that are GFP^+ (%)	$CDX2^+$ cells that are GFP^- (%)	$NANOG^-$ $CDX2^-$ cells (%)	$NANOG^-$ $CDX2^-$ cells that are GFP^+ (%)	$NANOG^-$ $CDX2^-$ cells that are GFP^- (%)
H2B-EGFP control	55	(68.15 ± 9.23)	(68.26 ± 10.81)	(68.17 ± 13.09)	(23.83 ± 6.71)	(22.33 ± 9.69)	(23.12 ± 11.92)
PRMT6CAN-OE	49	(68.86 ± 7.30)	(68.43 ± 11.97)	(69.34 ± 8.13)	(20.08 ± 7.32)	(20.18 ± 8.89)	(21.25 ± 8.62)
PRMT6MT2B2-OE	58	(69.07 ± 7.43)	(68.29 ± 9.89)	(69.91 ± 11.57)	(18.38 ± 7.13)	(19.46 ± 9.04)	(20.87 ± 10.24)

Data were represented as mean ± s.d. Wilcoxon signed-rank test with holm's adjustment were used for statistical analysis. Seven experimental replicates were performed.

Supplementary Table 4. Analysis of the distribution of progeny of siRNA injected two-cell blastomere at the blastocyst stage.

	Blastocysts 3D	Total cells (n)	$NANOG^+$ cells (%)	$CDX2^+$ cells (%)	GFP^+ cells (%)	$NANOG^+$ cells that are GFP^+ (%)	$NANOG^+$ cells that are GFP^- (%)	GFP^+ cells that are $NANOG^+$ (%)
siControl	37	77.62 ± 13.07	(10.41 ± 7.91)	(73.01 ± 7.94)	(49.20 ± 7.24)	(11.17 ± 13.49)	(9.79 ± 8.35)	(49.36 ± 31.70)
siPrmt6-1	29	70.79 ± 12.34	(11.74 ± 6.43)	(73.74 ± 7.99)	(44.19 ± 9.83)*	(14.40 ± 9.58)	(9.82 ± 7.47)	(54.58 ± 23.97)
siERVL-Prmt6	31	76.45 ± 12.63	(10.49 ± 4.93)	(70.13 ± 11.13)	(48.20 ± 7.26)	(11.23 ± 7.31)	(9.65 ± 6.19)	(49.52 ± 27.86)

Data were represented as mean ± s.d. Wilcoxon signed-rank test with holm's adjustment were used for statistical analysis, *$P < 0.05$. Three experimental replicates were performed.

Supplementary Table 5. Analysis of the cell fate distribution of *EGFP*, *Prmt6* ^{CAN} or *Prmt6* ^{MT2B2} mRNA injected one-cell embryos at the blastocyst stage.

	Blastcysts	Total cells (n)	NANOG^{+} cells (%)	CDX2^{+} cells (%)	NANOG^{-} CDX2^{-} cells (%)
EGFP control	39	77.49 ± 9.19	(15.50 ± 5.51)	(77.26 ± 6.07)	(9.62 ± 6.63)
Prmt6^{CAN}-OE	35	78.11 ± 10.15	(15.32 ± 6.98)	(73.85 ± 8.98)	(12.58 ± 7.54)
Prmt6^{MT2B2}-OE	34	78.21 ± 11.68	(14.34 ± 4.64)	(73.31 ± 8.16)*	(13.22 ± 8.59)*

Data were represented as mean ± s.d. Wilcoxon signed-rank test with holm's adjustment were used for statistical analysis, *P < 0.05. Three experimental replicates were performed.